ELSEVIER

Chemical Physics 217 (1997) 259–273

Chemical Physics

Vibronic and vibrational coherence and relaxation dynamics of molecules in condensed phases

M. Hayashi [a], T.-S. Yang [a], A. Mebel [a], C.H. Chang [a,b], S.H. Lin [a,b,c], N.F. Scherer [d]

[a] *Institute of Atomic and Molecular Sciences, Academia Sinica, Taipei, Taiwan, ROC*
[b] *Department of Chemistry, National Taiwan University, Taipei, Taiwan, ROC*
[c] *Department of Chemistry and Biochemistry, Arizona State University, Tempe, AZ 85287-1604, USA*
[d] *Department of Chemistry, University of Pennsylvania, Philadelphia, PA 19104-6332, USA*

Received 5 November 1996

Abstract

In this work, the effects of vibronic coupling competing with vibrational and/or vibronic relaxation on the femto-second pump–probe stimulated emission spectra of molecules in condensed phases are investigated theoretically. The femto-second pump–probe stimulated emission spectra are simulated as a function of temperature, excitation wavelength, and the energy gap and vibronic coupling constant between the relevant electronic states. We find that the vibronic transition depends on the excitation condition whether excitation occurs at higher or lower than the most probable transition level. Our simulation shows that even in non-equilibrium conditions a turn-over feature can be seen as a function of the energy gap between the vibronic states.

We also analyze the fs pump–probe experimental data of 1,1'3,3,3'3'-hexamethylindotricarbocyanine iodide (HITCI) in solutions. We find that vibrational coherence and its relaxation is the major contribution in the early stage after excitation.

1. Introduction

Ultra-short time-resolved spectroscopic measurements have shed light on ultra-fast molecular dynamics occurring in various materials ranging from semi-conductors to biological systems (for review [1]). One of the most important issues in the femtosecond study of molecules in such condensed media is the elucidation of the quantum mechanical role of the vibrational motions in facilitating vibronic transitions, electron transfer reactions and energy transfer processes.

Recently, a number of experiments have reported quantum beats in the time-resolved profiles of molecules in condensed phases opening a question whether non-equilibrated vibrational motions are important to relevant reactions or not [2–4]. In the theoretical aspect of this question, how fast vibrational relaxation occurs will be a criterion as to whether the assumption of thermal equilibrium is applicable or not [5,6]. If the relevant reaction takes place in non-equilibrium conditions, one should consider the transient vibrational and/or vibronic processes of the system.

Among such vibrational and/or vibronic processes, coherence transfer has drawn a great deal of attention [7–19]. Simulating the wave packet dynamics with the Markoff master equation, May et al. have studied a dissipative dynamics of a curve-crossing system [10–13]. To investigate the effects of vibrational coherence

PII S0301-0104(97)00016-5

transfer on the vibronic dynamics of a similar system, Jean and Fleming have performed quantum mechanical simulations [14]. From these studies, it has been shown that coherence transfer facilitates electronic curve crossing.

Quite recently, a more detailed study has been reported by Jean on the effect of vibrational coherence on electronic curve crossing [15]. It has been shown that interferences between coherent electronic and vibrational motion give rise to complex oscillatory feature in the electronic population dynamics. Ohtsuki and Fujimura have analytically derived the resonance condition for the bath-induced coherence transfer and shown numerically that the energy mismatch results in a strong reduction of the coherent transfer efficiency of the relevant system [8,9].

The multi-dimensionality and/or multi-level of a relevant system lead to difficulty in performing quantum mechanical simulations for dissipative systems. Pollad and Frisener, based on the density matrix formalism for a multi-level quantum model [5], carried out the calculation of the quantum dynamics of systems consisting of a number of levels [16]. Schneider et al. reported the dissipative electronic and vibrational dynamics of a multi-mode and multi-level system and showed that the multi-tuning modes result in a switch-over feature of the electronic population dynamics from coherent behavior to incoherent behavior [17]. Quite recently, Wolfseder and Domcke have applied the Monte Carlo wavefunction propagation method to the calculation of the quantum dynamics of a multi-mode vibronic coupling system with dissipation [18].

Solvent dynamics is also one of the central issues on how the solvent facilitates or controls the chemical processes. It becomes extremely important and interesting when the chemical process competes with solvent dynamics. Recently, the photophysics of dye molecules in solution has attracted intense experimental and theoretical attention [20–30]. For example, ultra-short time-resolved pump–probe measurements have been performed to investigate the vibrational dynamics of 1,1′3,3,3′3′-hexamethylindotricarbocyanine iodide (HITCI) in a variety of solvents [20]. The observed pump–probe profiles show quantum beats arising from the creation of the vibrational coherences of several modes. It is important to know the mechanism of how the vibrational and vibronic coherences and their relaxation affect the quantum beats of such a multi-mode system from the microscopic point of view, which, in turn, provides us a deeper understanding of the effects of solvent dynamics on the photo-induced molecular processes.

The purpose of this work is to provide the insight of how the vibrational and vibronic coherences and their relaxation processes affect the vibronic transitions between the relevant electronic states and, in turn, how these processes influence the quantum beats appearing in the fs time-resolved stimulated emission spectra. We have thus extensively studied the effects of vibronic coupling competing with vibrational and/or vibronic relaxation on the fs pump–probe stimulated emission spectra of molecules in condensed phases. We will show the effect of vibronic coupling constant, temperature, excitation wavelength, and the energy gap between the relevant electronic states on the fs pump–probe stimulated emission spectra.

In Section 2, we briefly describe a theoretical treatment of the fs pump–probe stimulated emission spectra, the coupled master equations for the vibrational population and vibrational and/or vibronic coherence dynamics, and microscopic expressions of the rate constants for these vibrational and vibronic processes. In Section 3, we perform numerical calculations to investigate the effect of vibronic coupling constant, temperature, excitation wavelength, and the energy gap between the relevant electronic states on the transient dynamics appearing in the spectra. Based on our theoretical treatment, we shall analyze fs pump–probe experimental data of HITCI in solutions.

2. Theory

2.1. Pump–probe time-resolved stimulated emission spectra

Here we consider a model for the pump–probe time-resolved measurement of a system with two vibronic manifolds $\{n\}$ and $\{m\}$ embedded in a heat-bath. The two vibronic manifolds are coupled by the interaction $\hat{H}'$.

A pumping laser excites the system from the ground vibronic manifold $\{g\}$ to the excited vibronic manifold $\{n\}$. After excitation, a probing laser is applied to induce transitions from the manifold $\{n\}$ to the manifold $\{g\}$ via stimulated emission and/or to higher excited manifolds via induced absorption. In this work, we shall focus on the pump–probe time-resolved stimulated emission experiment. In this case, an expression for the time-resolved profiles is derived in terms of the imaginary part of the transient susceptibility $\vec{\chi}''(\omega_{pu},\omega_{pr},\tau)$. In the adiabatic approximation and the Condon approximation, it has been shown that [22,31,32]

$$\vec{\chi}''(\omega_{pu},\omega_{pr},\tau) = -\sum_{n}\sum_{n'}\frac{\vec{\mu}_{ng}\otimes\vec{\mu}_{gn}}{\hbar}Re\{\rho_{nn'}(\omega_{pu},\tau)F_{nn'}(\omega_{pr})\}. \tag{1}$$

Here ω_{pu}, ω_{pr}, τ, and $\vec{\mu}_{ng}$ represent the central frequency of the pumping laser, that of the probing laser, the time interval between the two pulses, and the transition dipole moment, respectively and $F_{nn'}(\omega_{pr})$ is the band-shape function associated with the probing optical process. In Eq. (1), $\rho_{nn'}$ is the density matrix element of the molecular system after excitation by the pump pulse.

2.2. Relaxation and coherence dynamics

The Liouville equation for the density matrix $\hat{\rho}$ of the system in the absence of the radiation fields is given by [22]

$$\frac{d\hat{\rho}}{d\tau} = -i\hat{L}_0\hat{\rho} - \hat{\Gamma}\hat{\rho} - \frac{i}{\hbar}[\hat{H}',\hat{\rho}], \tag{2}$$

where $\hat{\Gamma}$ is the damping operator due to the interaction between the system and the heat bath.

By applying the adiabatic approximation and letting $\{g\} = (a,\{u\})$, $\{m\} = (b,\{v\})$, and $\{n\} = (c,\{w\})$ where, for example, $\{u\}$ represents the vibrational quantum numbers of the vibrational modes of the electronic ground state, the coupled master equations, for example, for $\rho_{bv,cw}$ can be written as

$$\frac{d\rho_{bv,cw}}{d\tau} = -(i\omega_{bv,cw} + \Gamma_{bv,cw})\rho_{bv,cw} - \sum_{v',w'}\Gamma_{bv,cw}^{bv',cw'}\rho_{bv',cw'} - \frac{i}{\hbar}\sum_{bv}\langle bv|J_{bc}(Q)|cw\rangle(\rho_{cw,cw} - \rho_{bv,bv})$$
$$-\frac{i}{\hbar}\left(\sum_{cw'=0}^{w'\neq w}\langle bv|J_{bc}(Q)|cw'\rangle\rho_{cw',bv} - \sum_{bv'=0}^{v'\neq v}\rho_{bv,bv'}\langle bv'|J_{bc}(Q)|cw\rangle\right), \tag{3}$$

where the vibronic dephasing rate constant for the vibronic coherence $bv \leftrightarrow cw$ is given by

$$\Gamma_{bv,cw} = -\sum_{v'\neq v,w'\neq w}\Gamma_{bv',cw'}^{bv,cw}.$$

We have assumed that the interaction Hamiltonian is given by $\hat{H}' = |c\rangle J_{cb}(Q)\langle b| + h.c.$ where Q denotes the normal coordinate. In the next section, we shall present a model of the relaxation processes.

2.3. A model of vibrational relaxation and dephasing

It has been found that the short-range interaction model can be applied to study the vibrational relaxation of molecules in condensed phases [33]. In this section, we shall apply this model to treat vibrational relaxation and pure dephasing in condensed phases. For this purpose, we apply the secular approximation to Eq. (3). This assumption allows one to focus on several important system–heat bath induced processes such as the vibrational population transition processes, the vibrational coherence transfer processes, and the vibronic processes.

Employing $\hat{V} = |b\rangle F_{1b}Q\exp(-\sum_j\alpha_j q_j)\langle b|$ as the system–heat bath interaction, where q_j denotes the vibrational coordiate of the j-th heat-bath mode, we obtain the vibrational population decay rate constant as [22,34]

$$\Gamma_{bv,bv} = \sum_{\Delta=\pm 1} W_{bv,bv+\Delta}, \tag{4}$$

where

$$W_{bv,bv+1} = e^{-\hbar\omega^b_{vib}/k_BT} W_{bv+1,bv} = (v+1)e^{-\hbar\omega^b_{vib}/k_BT}\gamma^b_{1\to 0}\,. \tag{5}$$

and

$$W_{bv,bv-1} = v\gamma^b_{1\to 0}\,. \tag{6}$$

Here $\gamma^b_{1\to 0}$ represents the vibrational relaxation rate constant for the transition $v=1\to v=0$ and is given by

$$\gamma^b_{1\to 0} = \frac{F^2_{1b}}{2\hbar\omega^b_{vib}}\int_{-\infty}^{\infty} dt \exp\{-it\omega^b_{vib}\}\exp\left[\sum_j S_j\left\{(1+2\bar{n}_j) + (1+\bar{n}_j)e^{it\omega_j} + \bar{n}_j e^{-it\omega_j}\right\}\right], \tag{7}$$

where $\hbar\omega_j$ denotes the one quantum energy of the j-th heat bath mode,

$$S_j = \frac{\alpha_j^2}{2\beta_j},\ \beta_j = \sqrt{\frac{\omega_j}{\hbar}} \text{ and } \bar{n}_j = (e^{\hbar\omega_j/k_BT}-1)^{-1}.$$

With the same interaction model used in Eq. (4), the vibrational relaxation rate constants associated with the vibrational population transitions $bv+1\to bv$ and $bv\to bv-1$ are given by

$$-\Gamma^{bv+1,bv+1}_{bv,bv} = (1+v)\gamma^b_{1\to 0} \tag{8a}$$

and

$$-\Gamma^{bv-1,bv-1}_{bv,bv} = ve^{-\hbar\omega^b_{vib}/k_BT}\gamma^b_{1\to 0}\,, \tag{8b}$$

respectively.

The rate constants of the vibrational coherence dynamics such as vibrational coherence transfer can be derived by using the same interaction model used in Eq. (4). For example, the rate constant of the vibrational coherence transfer process from $bv+1\leftrightarrow bv'+1$ to $bv\leftrightarrow bv'$ and from $bv-1\leftrightarrow bv'-1$ to $bv\leftrightarrow bv'$ is, respectively, given by

$$-\Gamma^{bv+1,bv'+1}_{bv,bv'} = \sqrt{v+1}\sqrt{v'+1}\,\gamma^b_{1\to 0} \tag{9a}$$

and

$$-\Gamma^{bv-1,bv'-1}_{bv,bv'} = \sqrt{v}\sqrt{v'}\exp(-\hbar\omega^b_{vib}/k_BT)\gamma^b_{1\to 0}\,. \tag{9b}$$

The pure dephasing rate constant can be derived by using the second order term with respect to the system variable and, for example, assuming $\hat{V} = \sum_{\lambda=b,c}|\lambda\rangle Q^2 F_{2\lambda}(\{q\})\langle\lambda|$ where $F_{2\lambda}(\{q\}) = F_{2\lambda}\exp(-\sum_j \alpha'_{\lambda j}q_j)$, we find the vibronic pure dephasing rate constant $D_{bv,cw}$ as

$$\begin{aligned} D_{bv,cw} = &\left(v+\frac{1}{2}\right)^2\gamma^{(d)}_b + \left(w+\frac{1}{2}\right)^2\gamma^{(d)}_c \\ &-\left(\frac{v+1/2}{\omega^b_{vib}}\right)\left(\frac{w+1/2}{\omega^c_{vib}}\right)\pi\hbar\sum_{\ell\ell'}P_\ell\langle\ell|F^2_b(\{q\})|\ell'\rangle\langle\ell'|F^2_c(\{q\})|\ell'\rangle\delta(E_{\ell'\ell}) \\ &-\left(\frac{v+1/2}{\omega^b_{vib}}\right)\left(\frac{w+1/2}{\omega^c_{vib}}\right)\pi\hbar\sum_{\ell\ell'}P_\ell\langle\ell|F^2_c(\{q\})|\ell'\rangle\langle\ell'|F^2_b(\{q\})|\ell'\rangle\delta(E_{\ell'\ell})\,. \end{aligned} \tag{10}$$

In the case of $\{\alpha'_{bj}\}\approx\{\alpha'_{cj}\}$, it follows that

$$D_{bv,cw} = \left(\frac{v+1/2}{\omega^b_{vib}} - \frac{w+1/2}{\omega^c_{vib}}\right)^2\pi\hbar\sum_{\ell}\sum_{\ell'}P_\ell|\langle\ell|F^2_b(\{q\})|\ell'\rangle|^2(E_{\ell'\ell})\,. \tag{11}$$

In the case in which the vibrational frequencies of the two electronic potentials are same, we find

$$D_{bv,cw} = (v - w)^2 \gamma_b^{(d)} \tag{12}$$

where

$$\gamma_b^{(d)} = \frac{F_{2b}^2}{2(\omega_{vib}^b)^2} \int_{-\infty}^{\infty} dt \exp\{it\omega_{vib}^b\} \exp\left[\sum_j S_j \left\{ (1 + 2\bar{n}_j) + (1 + \bar{n}_j) e^{it\omega_j} + \bar{n}_j e^{-it\omega_j} \right\} \right]. \tag{13}$$

In a similar manner, in the case of $\{\alpha'_{bj}\} \approx \{\alpha'_{cj}\}$ we can obtain the rate constant of the vibronic coherence transfer for $bv + 1 \leftrightarrow cw + 1$ to $bv \leftrightarrow cw$ as well. The vibrational pure dephasing rate constant is given by exchanging the subscripts cw (or bv) with bv' (or cw') in Eqs. (12) and (13).

Finally, we should note that the secular approximation allows us to omit the terms arising from the coherence creation or annihilation, i.e., for example, in Eq. (3) $\Gamma^{bv,cw}_{bv+1,cw-1}$ has been omitted.

3. Simulation and discussion

3.1. A single harmonic displaced oscillator mode system

We consider a model for a system consisting of the ground state manifold $\{au\}$ and the two electronically excited vibronic manifolds $\{bv\}$ and $\{cw\}$. To apply our theory to this system, these two electronically excited vibronic manifolds are coupled via vibronic coupling. We also assume that the pumping and probing lasers interacts only with the vibronic manifold $\{bv\}$ but not with $\{cw\}$. By applying the Condon approximation to the vibronic coupling terms in Eq. (5), i.e., $\langle bv|J_{bc}(Q)|cw\rangle \approx J_{bc}\langle bv|cw\rangle$, and by applying the secular approximation to the equations, we find

$$\begin{aligned}
\frac{d\rho_{bv,bv}}{d\tau} = & -\left[\left\{ v + (1+v) e^{-\hbar\omega_{vib}^b/k_B T} \right\} \gamma_{1\to 0} + \gamma_b \right] \rho_{bv,bv} \\
& + (1+v)\gamma_{1\to 0} \rho_{bv+1,bv+1} + v e^{-\hbar\omega_{vib}^b/k_B T} \gamma_{1\to 0} \rho_{bv-1,bv-1} \\
& - \frac{i}{\hbar} \sum_{cw=0} \left\{ J_{bc}\langle bv|cw\rangle \rho_{cw,bv} - \rho_{bv,cw} J_{cb}\langle cw|bv\rangle \right\},
\end{aligned} \tag{14}$$

$$\begin{aligned}
\frac{d\rho_{bv,bv'}}{d\tau} = & -(i\omega_{bv,bv'} + \Gamma_{bv,bv'} + \gamma_b)\rho_{bv,bv'} \\
& - \Gamma^{bv+1,bv'+1}_{bv,bv'} \rho_{bv+1,bv'+1} - \Gamma^{bv-1,bv'-1}_{bv,bv'} \rho_{bv-1,bv'-1} \\
& - \frac{i}{\hbar} \sum_{cw=0} \left\{ J_{bc}\langle bv|_{cw}\rangle \rho_{cw,bv'} - \rho_{bv,cw} J_{cb}\langle cw|bv\rangle \right\},
\end{aligned} \tag{15}$$

and

$$\begin{aligned}
\frac{d\rho_{bv,cw}}{d\tau} = & -\{i\omega_{bv,cw} + \Gamma_{bv,cw} + (\gamma_b + \gamma_c)/2\} \rho_{bv,cw} - \Gamma^{bv+1,bv'+1}_{bv,cw} \rho_{bv+1,cw'+1} - \Gamma^{bv-1,cw-1}_{bv,cw} \rho_{bv-1,cw-1} \\
& - \frac{i}{\hbar} \sum_{bv=0} \left(J_{bc}\langle bv|cw\rangle \rho_{cw,cw} - J_{cb}\langle cw|bv\rangle \rho_{bv,bv} \right) - \frac{i}{\hbar} \left(\sum_{cw'=0}^{w' \neq w} J_{bc}\langle bv|cw'\rangle \rho_{cw',cw} \right. \\
& \left. - \sum_{bv'=0}^{v' \neq v} \rho_{bv,bv'} J_{bc}\langle cw|bv'\rangle \right),
\end{aligned} \tag{16}$$

where, for example, J_{bc} and $\langle bv|cw\rangle$ represent the electronic coupling and the Franck–Condon overlap integrals, respectively. Here we have included in Eqs. (14)–(16) γ_b and γ_c as the radiative decay constant and/or the rate constant of non-radiative transitions other than the vibronic process of interest. Here the initial conditions of Eqs. (14) and (16) due to pumping are given in Appendix A and $\rho_{bv,cw}(\tau=0)=0$.

Now we are in a position to determine pump–probe stimulated emission spectra on the basis of Eqs. (14)–(16). For this purpose, we solve the coupled master equations numerically with the initial conditions given in Appendix A and then using Eq. (1) we can calculate pump–probe stimulated emission spectra. Notice that $F_{bv,bv'}(\omega_{pr})$ in Eq. (1) is also given in Appendix A. For numerical simulation, we employ the Runge–Kutta algorithm with a time step of 4 femtoseconds, and take from 7 to 16 vibrational states for each electronic state in order to achieve convergence of the numerical calculations.

First we shall investigate the vibronic coupling constant dependence of the pump–probe stimulated emission spectra. For this purpose, we set $\hbar\omega_{vib}\equiv\hbar\omega^a_{vib}=\hbar\omega^b_{vib}=\hbar\omega^c_{vib}=100\ \mathrm{cm}^{-1}$ and the Huang–Rhys factors are $S_{ba}=2.5$ for and $S_{cb}=1.0$, which are used for the Franck–Condon overlap integrals in Eqs. (14)–(16), (a1) and (a2). The excitation energy is chosen such that it is resonant to the most probable transition, i.e., $\hbar\omega_{pu}=\hbar\omega_{ba}+S_{ba}\hbar\omega_{vib}$. The vibrational relaxation rate constants are $\hbar\gamma_{1\to0}\equiv\hbar\gamma^a_{1\to0}=\hbar\gamma^b_{1\to0}=\hbar\gamma^c_{1\to0}=5.3\ \mathrm{cm}^{-1}$ and $\hbar\gamma^{(d)}\equiv\hbar\gamma^{(d)}_a=\hbar\gamma^{(d)}_b=\hbar\gamma^{(d)}_c=5.3\ \mathrm{cm}^{-1}$, and the radiative constant is $\hbar\gamma_r\equiv\hbar\gamma_b=\hbar\gamma_c=0.0053\ \mathrm{cm}^{-1}$. For the pumping and probing optical processes, we set $T_{pu}=T_{pr}=80$ fs and $\hbar\gamma_{pu}=\hbar\gamma_{pr}=66\ \mathrm{cm}^{-1}$. The temperature is set at 10 K.

Fig. 1 shows the spectra simulated for (a) the weak coupling case $\hbar J\equiv\hbar J_{bc}=\hbar J_{cb}=0.53\ cm^{-1}$, (b) the intermediate coupling case $\hbar J=1.3\ \mathrm{cm}^{-1}$, and (c) the strong coupling $\hbar J=5.3\ \mathrm{cm}^{-1}$ with the energy gap between the two electronic states b and c, $\hbar\omega_{bc}=100\ \mathrm{cm}^{-1}$. The spectra are shown as a function of the probing frequency and the time interval between the pump and probe processes.

The common characteristic of the quantum beats appearing in the calculated spectra for all cases is that the vibrational coherence is dominant after excitation and it lasts up to about $2\sim4$ ps. As the vibronic coupling constant becomes larger, the spectra shown in the panel (b) and (c) start decreasing their intensities after $2\sim4$ ps, while the spectra of the panel (a) shows a plateau feature. In the intermediate case, the vibronic transition takes place almost constantly. This is due to the fact that the vibronic coupling is not strong enough to transfer back the population from the electronic state c, compared with the vibrational relaxation process of the electronic state c. The situation is quite different in the strong coupling case. After the vibrational quantum beats disappear, new quantum beats take over in the spectra. The new oscillatory feature results from the creation of the vibronic coherence and shows a quite different phase relation versus the probe frequency, compared with the temporal behavior observed in the vibrational quantum beats.

This situation can be seen more clearly if the spectra are depicted in a counter map. Fig. 2 shows the comparison of the contour maps for the three cases. All the contour maps show in- and out-of phase relations within 2 ps as a function of the probing frequency. No out-of phase relations appear after $2\sim4$ ps in the panels (a) and (b), indicating the system reaches the vibrational equilibrium state. However, in the case (c) one can see the out-of phase relations disappear after 2ps although the spectra still show the quantum beats.

The behavior of the calculated spectra of the strong coupling case can easily be understood in terms of the vibrational population dynamics. Fig. 3 shows simulation of the population dynamics of the two vibronic manifolds. The populations $\rho_{bv,bv}(\tau)$ and $\rho_{cw,cw}(\tau)$ after excitation are calculated for (a) the weak coupling case and (b) the strong coupling case used in Fig. 1. The panel (b) in Fig. 3 clearly shows the population transfer between the two electronic states due to the creation of the vibronic coherence. Since all the vibrational population of the state b is transferred into $v=0$ if no population transfer takes place between the two electronic states, the time-resolved stimulated emission spectra forms a peak at $\hbar\omega_{pr}=\hbar\omega_{ba}-S_{ba}\hbar\omega_{vib}$. However, when the population of $v=0$ is transferred into the electronic state c the intensity of the spectra decreases showing its peak at $\hbar\omega_{pr}=\hbar\omega_{ba}-S_{ba}\hbar\omega_{vib}$.

It is informative to show how the vibrational motion of each electronic state evolves in time. For this purpose, we also demonstrate a wave packet representation of the density matrices $\rho_{b,b}(Q,\tau)$ and $\rho_{c,c}(Q,\tau)$ in

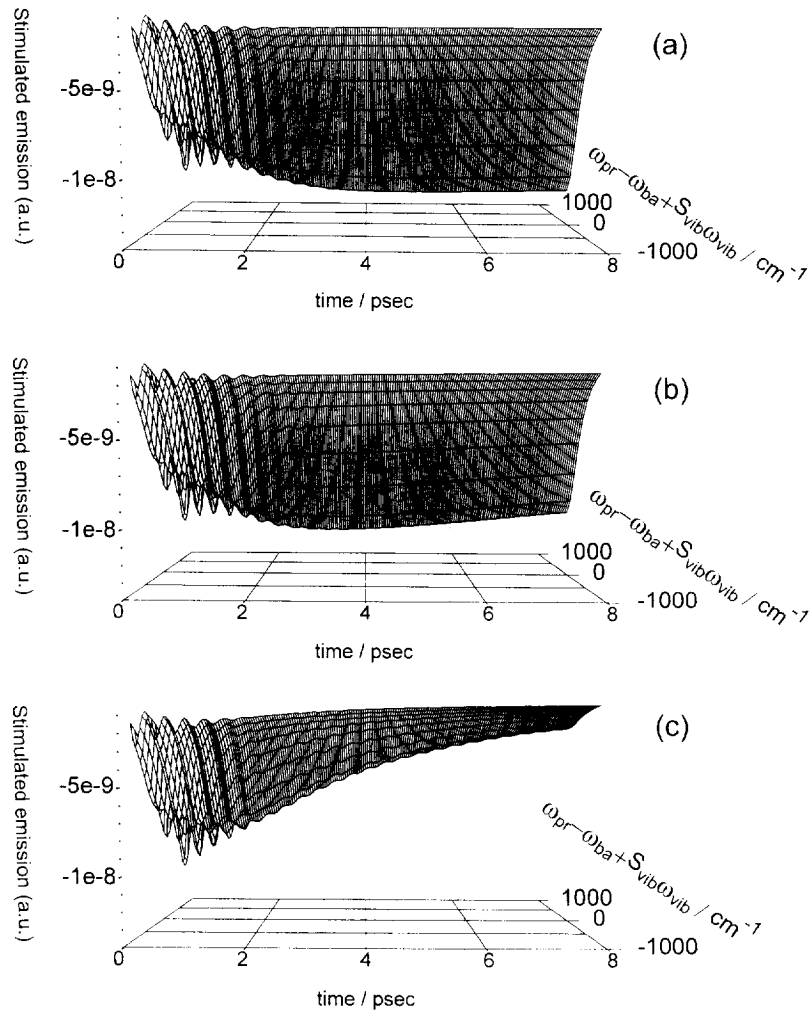

Fig. 1. Coupling constant dependence of the pump–probe stimulated emission spectra. The spectra are simulated for the cases: (a) the weak coupling $\hbar J = 0.53\ cm^{-1}$; (b) the intermediate coupling $\hbar J = 1.3\ cm^{-1}$; (c) the strong coupling $\hbar J = 5.3\ cm^{-1}$. The parameters used in the calculation are given in the text.

Fig. 4. The density matrices are calculated for the strong coupling case. The wave packets are obtained by transforming the density matrix in an energy representation to that in a normal mode coordinate representation. For example, $\rho_{b,b}(Q,\tau)$ is given by [6]

$$\rho_{b,b}(Q,\tau) = \sum_{v=0}^{\infty}\sum_{v'=0}^{\infty} \langle Q|bv\rangle\langle bv|\,\rho_{b,b}(\tau)|bv'\rangle\langle bv'|Q\rangle = \sum_{v=0}^{\infty}\sum_{v'=0}^{\infty} \rho_{bv,bv'}(\tau)\,\chi_{bv}(Q)\,\chi_{bv'}(Q) \qquad (17)$$

where

$$\chi_{bv}(Q) = \left(\frac{\sqrt{\beta_b/\pi}}{2^v v!}\right)^{1/2} H_{bv}\left(\sqrt{\beta_b}\,Q\right)\exp\left(-\beta_b Q^2/2\right),$$

$\beta_b = \omega_{\mathrm{vib}}^b/\hbar$ and $H_{bv}(\sqrt{\beta_b}\,Q)$ is Hermite polynomials.

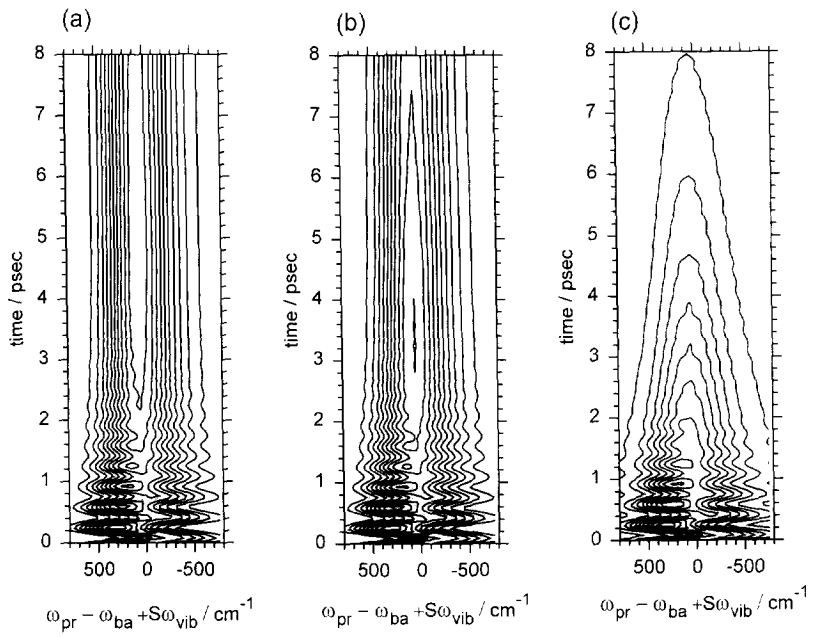

Fig. 2. A contour map representation of the calculated pump–probe stimulated emission spectra. The spectra are mapped for the cases: (a) the weak coupling; (b) the intermediate coupling; (c) the strong coupling. The calculated spectra are taken from Fig. 1.

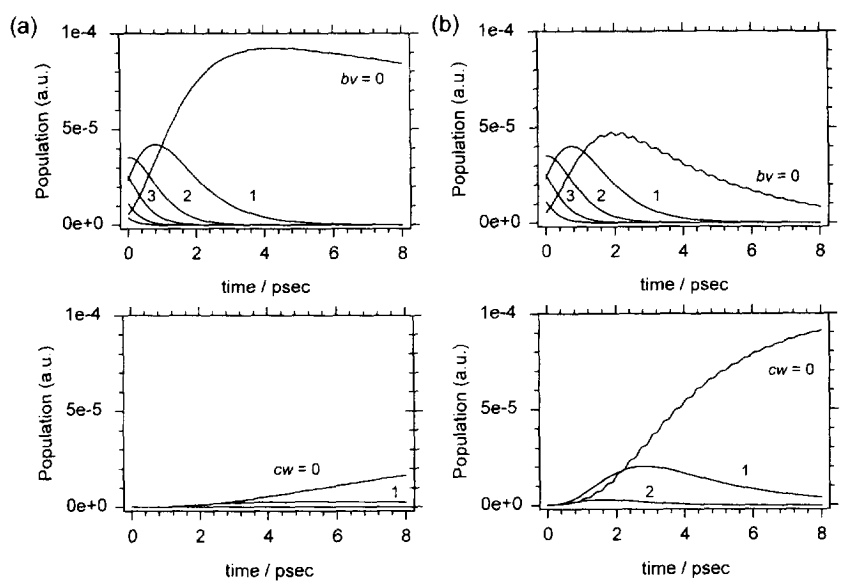

Fig. 3. Simulation of the population dynamics of the two vibronic manifolds after excitation. The populations $\rho_{bv,bv(\tau)}$ and $\rho_{cw,cw(\tau)}$ are calculated for (a) the intermediate coupling case $\hbar J = 1.3\ cm^{-1}$ and (b) the strong coupling case $\hbar J = 5.3\ cm^{-1}$. The excitation condition is the same as that used in Fig. 1. In each case, the upper and lower panels show the vibrational populations of the electronic states b and c, respectively.

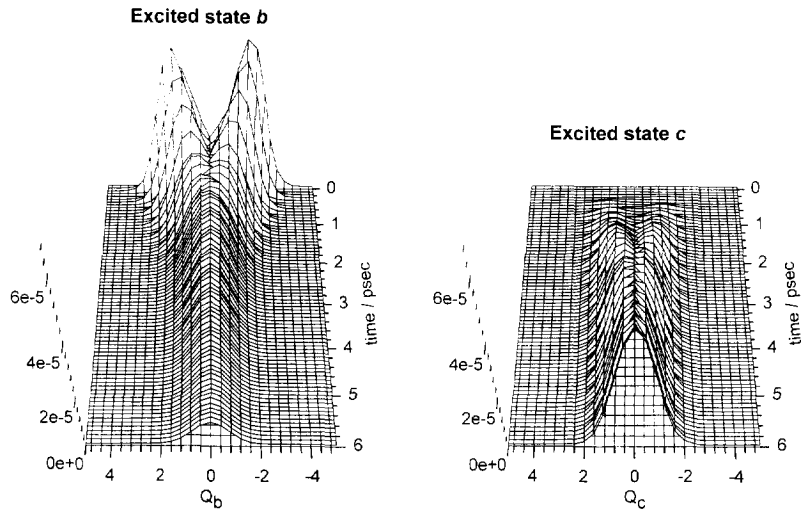

Fig. 4. A wave packet representation of the density matrices $\rho_{b,b}(Q,\tau)$ and $\rho_{c,c}(Q,\tau)$. The density matrix is calculated for the strong coupling case $\hbar J = 5.3\ cm^{-1}$. The wave packets are obtained on the basis of Eq. (17) with the calculated results used in the case (c) shown in Fig. 1.

Fig. 4 shows the motion of the wavepacket of the electronic state b and that of the electronic state c for the case (c) shown in Fig. 1. Within 2 ps, the wavepacket of the electronic state b is migrated on the harmonic potential surface losing its energy and coherence through the system-heat bath interaction and subsequently the motion stops, showing the vibrational wavefunction of the $v = 0$. The wavepacket of the electronic state c, on the other hand, forms around 1ps, showing a slight motion but not a large motion as seen in the electronic state b up to 2 ps. Since from the Huang–Rhys coupling constant we can see that the most probable transition takes place between $v = 0$ and $w = 1$, the dominant feature of the wavepacket of the electronic state c in the early time is the formation of the vibrational wavefunction of $w = 1$ on the potential surface of the electronic state c. The $w = 0$ character appears eventually due to the vibrational relaxation.

Now we shall investigate the excitation wavelength dependence of the pump–probe stimulated emission spectra. Fig. 5 shows the spectra simulated as a function of the pumping frequency at $\hbar\omega_{pu} = \hbar\omega_{ba}$. The rest of the parameters are the same as those used in Fig. 1. One can see in Fig. 5 that the quantum beats due to the

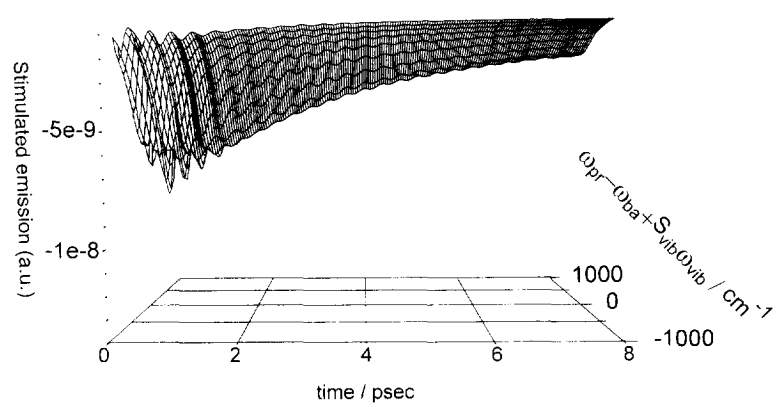

Fig. 5. Excitation wavelength dependence of the pump–probe stimulated emission spectra. The spectra are simulated at a pumping energy of $\hbar\omega_{pu} = \hbar\omega_{ba}$. The rest of the parameters used in the calculation are the same as those in the case (c) in Fig. 1 except for the excitation frequency.

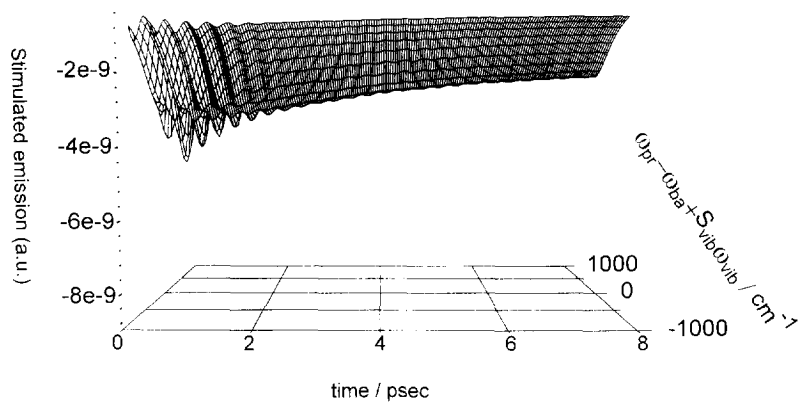

Fig. 6. Temperature dependence of the pump–probe stimulated emission spectra. The spectra are demonstrated as a function of temperature at $T = 300$ K. The rest of the parameters used in the calculation are the same as those in the case (c) shown in Fig. 1 except for the temperature.

vibrational coherence appear with in $2 \sim 3$ ps. Although compared with the ones in the panel (c) shown in Fig. 1, the intensity is smaller due to the off resonance effect, the temporal behaviors of the beats of both cases within $2 \sim 3$ ps are quite similar. The excitation condition, in this case, misses the vibrational level which undergoes the most probable vibronic transition to the electronic state c so that the vibronic transition will occur more slowly than the case in the panel (c) shown in Fig. 1. In fact, one can see that the intensity of the spectra around 8 ps is slightly higher than that shown in Fig. 1. When the pumping frequency is off-resonant but higher than the most probable transition vibrational level, it takes some more time for $v = 0$ to have considerable population via vibrational relaxation. In addition, in this case, secondary and tertiary probable transition paths are open to the population created at higher level via excitation.

Next we shall investigate the temperature dependence of the pump–probe stimulated emission spectra. The spectra are demonstrated as a function of temperatures at $T = 300$ K in Fig. 6. The rest of the parameters are the same as those employed in the case (c) shown in Fig. 1. Fig. 6 shows that the temperature effect destroys both vibrational and vibronic coherence. However, the quantum beats originated from the vibrational coherence are still a dominant feature in the early time region before 2 ps.

Finally we shall investigate the energy gap dependence of the pump–probe stimulated emission spectra. In Fig. 7, the spectra are simulated at various energy gaps of the two electronic states b and c, i.e., $\hbar\omega_{bc}$ = (a) 80; (b) 90; (c) 100; (d) 110; (e) 120; (f) 200; (g) 250; (h) 500 cm^{-1}. The parameters used in the calculations are the same as the case (c) shown in Fig. 1 except for the energy gap between the two electronic states.

Fig. 7 shows that the temporal behavior of each spectrum is almost identical, that is, the quantum beats appearing within 2 ps result from the vibrational coherence. Thus, they do not depend on the energy gap. However, the long time behavior of the spectra is quite different and interesting. The dynamics appearing in the calculated spectra depends strongly on the energy gap between the two electronic states. The calculated stimulated emission spectrum at $\hbar\omega_{bc} = 100$ cm^{-1} decreases its intensity most rapidly among the calculated spectra. As the energy gap becomes either larger or smaller than this condition, the intensities decrease slowly. This tendency can be explained in terms of the energy conservation and the Franck–Condon factor. Since for the Huang–Rhys factor $S_{bc} = 1$, the transition occurs most effectively when $\hbar\omega_{bc} = n\hbar\omega_{vib}$ where $n = 1$. As n increases, the Franck–Condon factor becomes smaller and the quantum beats due to the vibronic coherence disappear even for the case in which the energy is conserved.

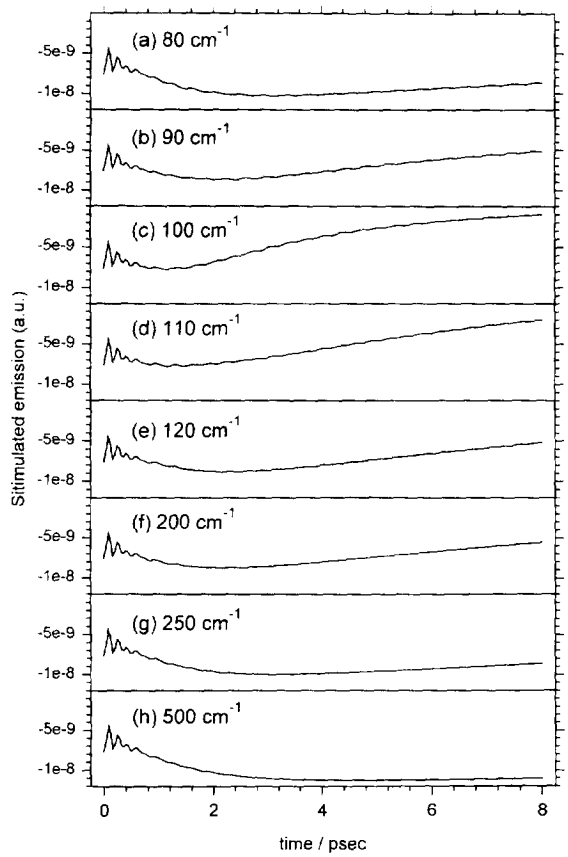

Fig. 7. Energy gap dependence of the pump–probe stimulated emission spectra. The spectra are simulated as a function of the energy gap: $\hbar\omega_{bc}$ = (a) 80; (b) 90; (c) 100; (d) 110; (e) 120; (f) 200; (g) 250; (h) 500 cm^{-1}. The parameters used in the simulation are the same as those for the case (c) shown in Fig. 1 except for the energy gap between the two electronic states b and c.

3.2. Application to the analysis of experimental femtosecond pump–probe spectra of a multi-dimensional system

Recently, fs time-resolved measurements have been performed for 1,1'3,3,3'3'-hexamethylindotricarbocyanine iodide (HITCI) in various solvents with laser pulses of a few ten femtoseconds [20]. The observed spectra show quantum beats arising from the excitation of several vibrational modes and also exhibit non-exponential decays with time constants of about sub-picoseconds and several picoseconds.

In this sub-section, we shall attempt to apply our theoretical treatment to investigate the dynamics appearing in the observed spectra of this multi-dimension vibrational (i.e. multi-mode) system, that is, we would like to know how fast the vibrational relaxation is and how multi-mode excitation affects coherence dynamics. For this purpose, we shall consider a two-mode model and employ the short time excitation approximation for the pumping process in which the vibrational coherences between the electronic ground state and excited state are created. The latter assumption allows us to ignore the off-diagonal (or secular) terms associated with the

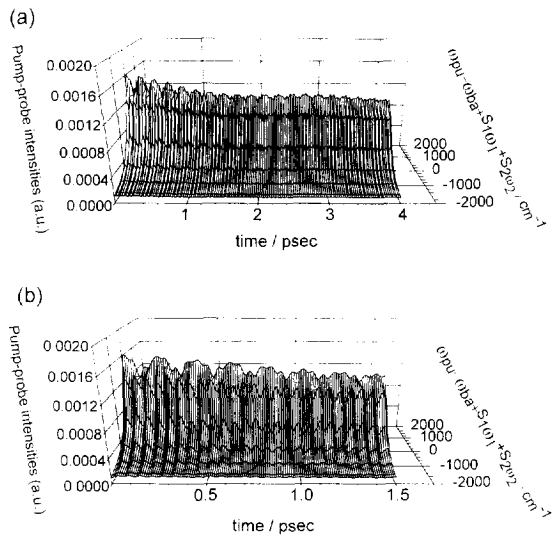

Fig. 8. The calculated pump–probe stimulated emission spectra of the multi-dimensional system. The simulations are performed for (a) the long time region and (b) the short time region.

vibronic relaxation processes in the master equation for the pumping process, and to factorize the initial condition into a product of each mode. In this case, under the Franck–Condon approximation we find

$$\rho_{bv,bv'}(T_{\rm pu}) = \frac{T_{\rm pu}^2}{\hbar^2}\left\{\vec{\mu}_{b,a}\cdot\vec{E}_{\rm pu}(\omega_{\rm pu})\right\}\left\{\vec{\mu}_{b,a}\cdot\vec{E}_{\rm pu}(-\omega_{\rm pu})\right\}\prod_{j=1}^{2}\sum_{au'_j=0} P_{au'_j}\langle bv_j|au'_j\rangle\langle au'_j|bv'_j\rangle . \tag{18}$$

For performing the simulation, we set $\hbar\omega_1 \equiv \hbar\omega_1^a = \hbar\omega_1^b = \hbar\omega_1^c = 160\ \mathrm{cm}^{-1}$ and the Huang–Rhys factors are $S_{1ab} = 0.4$ and $S_{1cb} = 0.2$ for the low frequency mode, and $\hbar\omega_2 \equiv \hbar\omega_2^a = \hbar\omega_2^b = \hbar\omega_2^c = 550\ \mathrm{cm}^{-1}$ and the Huang–Rhys factors are $S_{2ab} = 0.11$ and $S_{2cb} = 0.1$ for the high frequency mode. The energy gap between the two electronic states is set to be $\hbar\omega_{\rm bc} = 170\ \mathrm{cm}^{-1}$. The vibrational relaxation and dephasing rate constants are $\hbar\gamma_{1\to 0}^{1} \equiv \hbar\gamma_{1\to 0}^{a1} = \hbar\gamma_{1\to 0}^{b1} = \hbar\gamma_{1\to 0}^{c1} = 5.3\ \mathrm{cm}^{-1}$, $\hbar\gamma_1^{(\rm d)} \equiv \hbar\gamma_{1a}^{(\rm d)} = \hbar\gamma_{1b}^{(\rm d)} = \hbar\gamma_{1c}^{(\rm d)} = 1.3\ \mathrm{cm}^{-1}$, and $\hbar\gamma_2^{(\rm d)} \equiv \hbar\gamma_{2a}^{(\rm d)} = \hbar\gamma_{2b}^{(\rm d)} = \hbar\gamma_{2c}^{(\rm d)} = 0.66\ \mathrm{cm}^{-1}$. The radiative constant is $\hbar\gamma_{\rm r} \equiv \hbar\gamma_b = \hbar\gamma_c = 0.0053\ \mathrm{cm}^{-1}$. For the probing processes, we set $T_{\rm pr} = 20$ fs and $\hbar\gamma_{\rm pu} = \hbar\gamma_{\rm pr} = 265\ \mathrm{cm}^{-1}$. The temperature is set at 300 K. We take from 4 to 6 vibrational states for the 170 cm^{-1} mode and 2 states for the 550 cm^{-1}. The time step are taken to be 1 fs and 2.67 fs for the short and long time simulations, respectively.

Fig. 8 shows the calculated pump–probe stimulated emission spectra of the two dimensional system. From the panel (a), we can see the temporal behavior of the spectra at the maximum intensity shows two oscillatory components, accompanying with two decay components whose time constants are about 300 fs and 200 ps. Up to 2ps, the low frequency mode retains coherence, resulting in a slight movement in the time-resolved spectra versus the probing frequencies. One can clearly see the short time behavior in the panel (b) in Fig. 8. Since the Huang–Rhys factor for the low frequency mode is small, the most probable transition takes place to $\nu = 0$. From around 3 ps, the maximum intensity shows a slow decay resulting from the vibronic transition to the other electronic state.

From this simulation, we can see that at least within the early time region after excitation, vibrational coherence and its relaxation are the main contribution to the spectra and then most of the population are accumulated at $\nu = 0$; vibronic transition then becomes dominant.

A more quantitative discussion based on ab-initio calculation for the vibrational frequencies and their displacements of HITCI and solvent effects on the fs time-resolved spectra will be reported later.

4. Summary

We have investigated the effects of the vibronic coupling competing with vibrational and/or vibronic relaxation on the fs pump–probe stimulated emission spectra of molecules in condensed phases. Taking into account vibronic and vibrational relaxation and vibronic coupling, we briefly derive the coupled master equations for the vibrational population and vibrational and/or vibronic coherence dynamics. Microscopic expressions of the rate constants for these vibrational and vibronic processes are obtained by employing a short-range interaction model. By simulating the coupled master equations, we have studied the effect of vibronic coupling constant, temperature, excitation wavelength, and the energy gap between the relevant electronic states on the transient dynamics appearing in the spectra.

Although our numerical approach to the coupled master equations are quite similar to those reported by Jean [15,35] and collaborators [14] and May and collaborators [10–13], our emphasis is mostly placed on showing how vibrational and vibronic coherences are reflected in the pump–probe time-resolved stimulated emission spectra. Most of the distinctive features due to vibrational and vibronic coherences were also seen in these works. However, in the present work, we have shown that a turn-over feature can be seen in vibronic dynamics appearing in the calculated pump–probe stimulated emission spectra as a function of the energy gap between the two relevant vibronic states. We have found that vibronic quantum beats cannot be observed when the energy gap becomes larger in which situation it leads to smaller Franck–Condon overlaps between the energy conserved levels.

To see the essence of the ultra-fast dynamics occurring in multi-dimensional system at room temperature, we have attempted to analyze fs pump–probe experimental data of HITCI in a liquid phase. We have shown that vibrational coherence and its relaxation are most likely to be the main contribution to the spectra within the early time region after excitation, and then vibronic transition becomes dominant.

Finally, it should be noted that the importance of studying the quantum dynamics of multi-mode and multi-level systems was also emphasized by Friesner et al. [5,16] and Domcke et al.[17,18]. More rigorous quantum mechanical simulation techniques have been developed and extended by these groups.

Acknowledgements

This work was supported by NSC of the Republic of China. We would like to thank the referees for helpful comments and suggestions.

Appendix A

The initial condition for the vibrational coherence $\rho_{bv,bv'}$ can be obtained by the second order approximation with respect to the system–laser interaction due to the pumping laser. Notice that in the Franck–Condon approximation, we obtain [22,31,32]

$$\rho_{bv,bv'}(\tau=0)=\frac{1}{\hbar^2}\sum_{au'}\rho_{au',au'}\left\{\vec{\mu}_{b,a}\cdot\vec{E}_{\mathrm{pu}}(\omega_{\mathrm{pu}})\right\}\left\{\vec{\mu}_{a,b}\cdot\vec{E}_{\mathrm{pu}}(-\omega_{\mathrm{pu}})\right\}\langle bv|au'\rangle\langle au'|bv'\rangle$$
$$\times\left[\frac{1}{\omega_{bv',au'}+\mathrm{i}\Gamma_{bv',au'}-\omega_{\mathrm{pu}}+\mathrm{i}\gamma_{\mathrm{pu}}+\mathrm{i}\gamma_b/2}\left\{\frac{1-\mathrm{e}^{-\mathrm{i}T_{\mathrm{pu}}(\omega b_{\cdot,b\cdot}-\mathrm{i}\Gamma_{b\cdot,b\cdot}-\mathrm{i}\gamma_b)}}{\omega_{bv,bv'}-\mathrm{i}\Gamma_{bv,bv'}-\mathrm{i}\gamma_b}\right.\right.$$
$$\left.\left.-\frac{\mathrm{e}^{\mathrm{i}T_{\mathrm{pu}}(\omega_{b\cdot,au'}+\mathrm{i}\Gamma_{b\cdot,au'}-\omega_{\mathrm{pu}}+\mathrm{i}\gamma_{\mathrm{pu}}+\mathrm{i}\gamma_b/2)}-\mathrm{e}^{-\mathrm{i}T_{\mathrm{pu}}(\omega_{b\cdot,b\cdot}-\mathrm{i}\Gamma_{b\cdot,b\cdot}-\mathrm{i}\gamma_b)}}{\omega_{bv',au'}+\omega_{bv,bv'}+\mathrm{i}\Gamma_{bv',au'}-\mathrm{i}\Gamma_{bv,bv'}-\omega_{\mathrm{pu}}+\mathrm{i}\gamma_{\mathrm{pu}}-\mathrm{i}\gamma_b/2}\right\}\right]$$

$$-\frac{1}{\omega_{bv,au'}-i\Gamma_{bv,au'}-\omega_{pu}-i\gamma_{pu}-i\gamma_b/2}\left\{\frac{1-e^{-iT_{pu}(\omega_{bt,bt'}-i\Gamma_{bt,bt'}-i\gamma_b)}}{\omega_{bv,bv'}-i\Gamma_{bv,bv'}-i\gamma_b}\right.$$

$$\left.-\frac{e^{iT_{pu}(\omega_{au',bt}+\omega_{pu}+i\gamma_{pu}+i\gamma_b/2)}-e^{-iT_{pu}(\omega_{bt,bt'}-i\Gamma_{bt,bt'}-i\gamma_b)}}{\omega_{bv,au'}+\omega_{bv,bv'}+i\Gamma_{bv,au'}-i\Gamma_{bv,bv'}+\omega_{pu}+i\gamma_{pu}-i\gamma_b/2}\right\}. \tag{a1}$$

In a similar manner, $F_{bv,bv'}(\omega_{pr})$ is given by [22,31,32]

$$F_{bv,bv'}(\omega_{pr})=\sum_{au=0}\langle bv'|au\rangle\langle au|bv\rangle\left[\frac{1}{\omega_{bv',au}+\omega_{bv,bv'}+i\Gamma_{bv',au}-i\Gamma_{bv,bv'}-\omega_{pu}+i\gamma_{pu}-i\gamma_b/2}\right.$$

$$\times\left\{\frac{1-e^{-iT_{pu}(\omega_{bt,bt'}-i\Gamma_{bt,bt'}-i\gamma_b)}}{\omega_{bv,bv'}-i\Gamma_{bv,bv'}-i\gamma_b}+\frac{1-e^{iT_{pr}(\omega_{bt',au}+i\Gamma_{bt',au}-\omega_{pu}+i\gamma_{pu}+i\gamma_b/2)}}{\omega_{bv',au}+i\Gamma_{bv',au}-\omega_{pr}+i\gamma_{pu}+i\gamma_b/2}\right\}$$

$$-\frac{1}{\omega_{bv,au}+\omega_{bv,bv'}-i\Gamma_{bv,au}+i\Gamma_{bv,bv'}-\omega_{pu}-i\gamma_{pu}+i\gamma_b/2}$$

$$\left.\times\left\{\frac{1-e^{-iT_{pu}(\omega_{bt,bt'}-i\Gamma_{bt,bt'}-i\gamma_b)}}{\omega_{bv,bv'}-i\Gamma_{bv,bv'}-i\gamma_b}+\frac{1-e^{iT_{pr}(\omega_{bt,au}+i\Gamma_{bt,au}-\omega_{pu}+i\gamma_{pu}+i\gamma_b/2)}}{\omega_{bv,au}+i\Gamma_{bv,au}-\omega_{pr}+i\gamma_{pu}+i\gamma_b/2}\right\}\right], \tag{a2}$$

where ω_{pu} (T_{pu} and γ_{pu}) and ω_{pr} (T_{pr} and γ_{pr}) represent the central frequency of the pumping laser (its time duration and coherency) and that of the probing laser (its time duration and coherency), respectively.

References

[1] Ultrashort Laser Pulses Generation and Applications Second edition in Topics in Applied Physics, ed. W. Kaiser (Spring-Verlag, 1993, Berlin).
[2] M.H. Vos, F. Rappaport, J.C. Lambry, J. Breton and J.-L. Martin, Nature 363 (1993) 320.
[3] M.H. Vos, M.R. Jones, C.N. Hunter, J. Breton, J.-C. Lambry, J. Breton and J.-L. Martin, Biochemistry 33 (1994) 6750.
[4] K. Wynne, C. Galli and R.M. Hochstrasser J. Chem. Phys. 100 (1994) 4797.
[5] J.M. Jean, R. Friesner and G.R. Fleming J. Chem. Phys. 96 (1992) 5827.
[6] M. Sugawara, M. Hayashi, S. Suzuki and S.H. Lin, Mol. Phys. 87 (1996) 637.
[7] P. de. Bree and D.A. Wiersma, J. Chem. Phys. 70 (1979) 790.
[8] Y. Ohtuski and Y. Fujimura, J. Chem. Phys. 91 (1989) 3903.
[9] Y. Ohtuski and Y Fujimura, J. Chem. Phys. 104 (1996) 8321.
[10] V. May, O. Kühn and M. Schreiber, J. Phys. Chem. 97 12591 (1993)
[11] O. Kühn, V. May and M. Schreiber, J. Chem. Phys. 101 (1994) 10404.
[12] O. Kühn, D. Malzahn and V. May, Intern. J. Quant. Chem. 57 (1996) 343.
[13] V. May and M. Schreiber, Phys. Rev. A 45 (1992) 2826.
[14] J.M. Jean and G.R. Fleming, J. Chem. Phys. 103 (1995) 2092.
[15] J.M. Jean, J. Chem. Phys. 104 (1996) 5638.
[16] W.T. Pollard and R.A. Friesner, J. Chem. Phys. 100 (1994) 5054.
[17] R. Schneider, W. Domcke and H. Köppel, J. Chem. Phys. 92 (1990) 1045.
[18] B. Wolfseder and W. Domcke, Chem. Phys. Lett. 245 (1995) 370.
[19] I. Martini and G.V. Hartland, Chem. Phys. Lett. 258 (1996) 180.
[20] P. Vöhringer, R.A. Westervelt, T.-S. Yang, D.C. Arnett, M.J. Feldstein and N.F. Scherer, J. Raman. Spectrosc. 26 (1995) 535.
[21] Y. Gaudual and P. Rossky, eds., Ultrafast Reaction Dynamics and Solvent Effects (AIP, New York, 1993).
[22] S.H. Lin, R.G. Alden, R. Islampour, H. Ma and A.A. Villaeys, Density Matrix Method and Femtosecond Processes (World Scientific, Singapore, 1991).
[23] S. Mukamel, Ann. Rev. Phys. Chem. 41 (1990) 647.

[24] R.F. Loring, Y.J. Yan and S. Mukamel, J. Chem. Phys. 87 (1987) 5840.
[25] I.A. Walmsley, M. Mitsunaga and C.L. Tang, Phys. Rev. A38 (1988) 4681.
[26] U. Banin and S. Ruhman, J. Chem. Phys. 98 (1993) 4391.
[27] N.F. Scherer, L.D. Ziegler and G.R. Fleming, J. Chem. Phys. 96 (1992) 5544.
[28] N.F. Scherer, D.M. Jonas and G.R. Fleming, J. Chem. Phys. 99 153 (1993).
[29] D.W. Oxtoby and S.A. Rice, Chem. Phys. Lett. 42 (1976) 1
[30] D.W. Oxtoby, Adv. Chem. Phys. 47 (1981) 487.
[31] B. Fain, S.H. Lin and N. Hamer, J. Chem. Phys. 91 (1989) 4485.
[32] S.H. Lin, B. Fain and N. Hamer, Adv. Chem. Phys. 79 (1990) 133.
[33] H. Eyring, S.H. Lin and S.M. Lin, Basic Chemical Kinetics (Wiley-Interscience, New York, 1980).
[34] Y. Fujmura, in: Advances in Multi-photon Processes and Spectroscopy, ed. S.H. Lin (World Scientific, Singapore, 1986) Vol. 2, p. 1.
[35] J.M. Jean, J. Chem. Phys. 101 (1994) 10464.